Research Square

Preprints are preliminary reports that have not undergone peer review.
They should not be considered conclusive, used to inform clinical practice,
or referenced by the media as validated information.

Stage-Dependent Topographical and Optical Properties of Plasmodium Falciparum-Infected Red Blood Cells

Katharina Preißinger (katharina.preissinger@physik.uni-augsburg.de)
University of Augsburg
Beáta Vértessy
BME
István Kézsmárki
University of Augsburg
Miklós Kellermayer
Semmelweis University
Petra Molnár
BME

Research Article

Keywords: Malaria, Intraerythrocytic cycle, Plasmodium falciparum, hemozoin crystals, RBCs

Posted Date: June 2nd, 2021

DOI: https://doi.org/10.21203/rs.3.rs-568282/v1

License: This work is licensed under a Creative Commons Attribution 4.0 International License.
Read Full License

Stage-dependent topographical and optical properties of *Plasmodium falciparum*-infected red blood cells

Katharina Preißinger[1,2,3,4,*], Petra Molnár[1,2,3], Beáta Vértessy[1,2], István Kézsmárki[3,4], and Miklós Kellermayer[5]

[1]Department of Applied Biotechnology and Food Sciences, BME, 1111 Budapest, Hungary
[2]Institue of Enzymology, research Center for Natural Sciences, 1111 Budapest, Hungary
[3]Department of Physics, BME, 1111 Budapest, Hungary
[4]Department of Experimental Physics V, University of Augsburg, 86159 Augsburg, Germany
[5]Department of Biophysics and Radiation Biology, Semmelweis University, 1111 Budapest, Hungary
[*]katharina.preissinger@physik.uni-augsburg.de

ABSTRACT

Efficient malaria treatment is a major healthcare challenge. Addressing this challenge requires in-depth understanding of malaria parasite maturation during the intraerythrocytic cycle. Exploring the structural and functional changes of the parasite through the intraerythrocytic stages and their impact on red blood cells (RBCs) is a cornerstone of antimalarial drug development. In order to precisely trace such changes, we performed a thorough imaging study of RBCs infected by *Plasmodium falciparum*, by using atomic force microscopy (AFM) and total internal reflection fluorescence microscopy (TIRF) supplemented with bright field microscopy for stage assignment. This multifaceted imaging approach allows to reveal structure–function relations via correlations of the parasite maturation with morphological and fluorescence properties of the stages. We established diagnostic patterns characteristic to the parasite stages based on the topographical profile of infected RBCs, which show close correlation with their fluorescence (TIRF) map. Furthermore, we found that hemozoin crystals exhibit a strong optical contrast, possibly due to the quenching of fluorescence. The topographical and optical features provide a tool for locating the hemozoin crystals within the RBCs and following their growth.

Introduction

Every year, more than 200 million people are infected with malaria. Five species of the *Plasmodium* genus cause human malaria infection, among which *P. falciparum* and *P. vivax* are the most widespread and mainly responsible for severe malaria[1]. The protozoon is transmitted into the human body by mosquito bite. Following the liver stage, an asexual cycle of the parasites takes place in the blood stream: RBCs are invaded by merozoites. The parasites then mature into rings, trophozoites and finally to schizonts. Subsequently they multiply, burst out of the host cell and begin the next cycle by invading new RBCs. This intraerythrocytic cycle has been the subject of intense research because it causes the main clinical symptoms. Therefore, the intraerythrocytic cycle has become the major target of antimalarial treatment and diagnostics. The digestion of hemoglobin by all *Plasmodium* species results in the accumulation of a micro-crystalline metabolic byproduct, called hemozoin, leading to morphological changes of the RBC. These alterations provide a solid basis for the standard bright-field microscopy (BFM) diagnostic detection[2,3] of malaria, and have raised the possibility of alternative diagnostic methods such as magneto-optical techniques[4–7]. The development of a cavity associated with early-ring forms was observed within the RBCs[8], which spreads and extends in late rings. Towards the trophozoite stage, when a considerable portion of the hemoglobin has already been transformed, hemozoin becomes concentrated into co-aligned crystals within a single food vacuole of the parasite. During the trophozoite stage, the vacuole is settled to the side of the parasite, while growing further in size. The prominent cavity disappears during maturation to the schizont stage. The maturation steps are presumably associated with alterations in the external morphology and mechanical properties of the RBCs, which are little understood.

By using AFM on *P. falciparum*-infected RBCs, Nagao E. *et al.* were able to correlate structural alterations with developmental stages of the parasite and determine their position inside the cell[9]. A closer investigation of the cytoskeleton of the infected RBC showed a correlation between changes in mechanical properties and alterations in cell morphology[10]. By combining IR-spectroscopy with AFM, Perez-Guaita D. *et al.* provided maps to resolve chemical and topographical information about infected RBCs without the need for contrast materials[11]. In addition to topographical characteristics, the fluorescence

spectral features of malaria-infected blood samples[12] revealed distinct differences between infected and healthy RBCs. Their spectral analysis at an excitation wavelength of 400 nm showed characteristic fluorescence bands for chemical compounds, e.g. porphyrin, inside the RBCs. A further study of human blood samples with laser-induced autofluorescence by Opoku-Ansah *et al.*[13] revealed higher mean fluorescence intensity for healthy RBCs compared with *P. falciparum*-infected ones. The authors presumed that the lower fluorescence intensity observed in the infected cells was caused by the quenching of fluorescence by hemozoin.

In order to explore *Plasmodium*-induced morphological and mechanical changes of infected RBCs, we combined AFM[9–11,14,15] and TIRF[16]. This comparative analysis, carried out on a large number of RBCs containing ring, trophozoite and schizont forms, allowed to correlate the morphological changes of RBCs with the *P. falciparum* developmental stages, which were staged by BFM. We could establish a correlation between typical RBC topographical profiles and *Plasmodium* development stages. Our analysis provides basis for an AFM-based identification of the parasites stages without the need for contrast materials, which is a clear advantage with respect to most of the methods commonly used for the classification of malaria developmental stages, such as BFM microscopy on Giemsa-stained smears[17], Polymerase Chain Reaction (PCR)[18] and flow cytometry[19].

Results

Morphological changes in infected RBCs

In the following, we analyse the influence of the parasite maturation on the topography of RBCs. Furthermore, we explore how this information can be used to classify the stages according to characteristic parameters. In this work, we carried out a systematic AFM study on various Giemsa-stained thin film smears of synchronized *P. falciparum* cultures, which were characteristic for the different developmental stages. The stages —ring, trophozoite and schizont— were determined by BFM, as shown by representative images in the first row of Fig. 1. Healthy RBCs show almost no surface deflection and appear as nearly flat in their partially dehydrated form within the smear (Fig. 1a). In the ring stage, a cavity at the position of the ring, typically close to the centre of infected RBCs, was detected. We found that this cavity is the hallmark of the ring-stage of the *Plasmodium* intra-erythrocyte cycle, which is clearly resolved in the corresponding topography image in Fig. 1b. Upon maturation to the trophozoite stage, the cavity widened, occupying up to half of the cell diameter and moving slightly off-centre (see Fig. 1c). The topography in the schizont stage (Fig. 1d) reflects another radical transformation. The surface of the RBC becomes flat and featureless again, similarly to the healthy one, albeit displaying distinct roughness. In addition, the contour of the cell is less regular, in stark contrast with the nearly cylindrical shape of the uninfected RBC and the early stages.

To quantitatively characterise the topographical structure of the RBC, we extracted height profiles along an arbitrary number of cross-sections through the centre of the cell with a custom-developed python program (Evaluation program). In the present study, we defined 18 radial cross-sections, so that a profile plot was obtained every 10° around an RBC (Fig. 1a, top panel). The ensemble of height profiles for the respective AFM image of example RBCs for the developmental stages (Fig. 1, second row) are shown in the third row of Fig. 1. Notably, with the exception of the trophozoite stage, the height profiles are symmetric with respect to the centre of the cell. It is also clear that the height shows small variations along the radius for uninfected cells and schizonts, while it exhibits a large drop in rings and trophozoites, when approaching the cell centre from the periphery. Averaging these height profiles for a given cell reveals the radial dependence of the height, as seen in the bottom row of Fig. 1.

In the average height profiles of the different stages, we can recognize the typical features already noticed in the 2D images: The flat discoid shape of the uninfected RBC[20], the central cavity signalling the ring stage[8] and the nearly featureless landscape with reduced overall height, characteristic to the schizont stage. This statistical difference in the radial profiles allows for staging of malaria infection. However, by averaging we loose the information about the asymmetry of the cells, arising e.g. from the off-centring of the parasites, which is particularly important for trophozoites. This information can be recovered from the standard deviation of the height, as represented by the shaded area around the average curve. This deviation is not solely determined by the overall asymmetry of the height profiles, but short-scale surface roughness can also contribute to it. The deviation is the largest for the trophozoite stage and increases gradually from the periphery to the centre, which implies the primary role of asymmetry in the deviation of the height. In the following, we will show that these morphological features are not specific to the exemplary cells displayed in Fig. 1, but characteristic to the different stages.

For further analysis, we sorted all topography images according to the parasite stages into the four categories —uninfected RBC, ring, trophozoite, schizont— using BFM. In order to identify key differences between the different stages, the radial height profiles were determined for every cell by the averaging process described above. Then, these radial height profiles were averaged for all cells of the same stage (approx. 100 cells for each stage) to obtain a master curve describing the typical morphology of that stage. These master curves, shown in Fig. 2, reproduce the key features observed for individual cells of the corresponding stage (see Fig. 1).

The mean height h_{mean} is nearly the same for the uninfected RBC and for the ring stage, while it shows a significant reduction in the trophozoite and schizont stages. More interestingly, the height drop from the maximum at the cell edge to

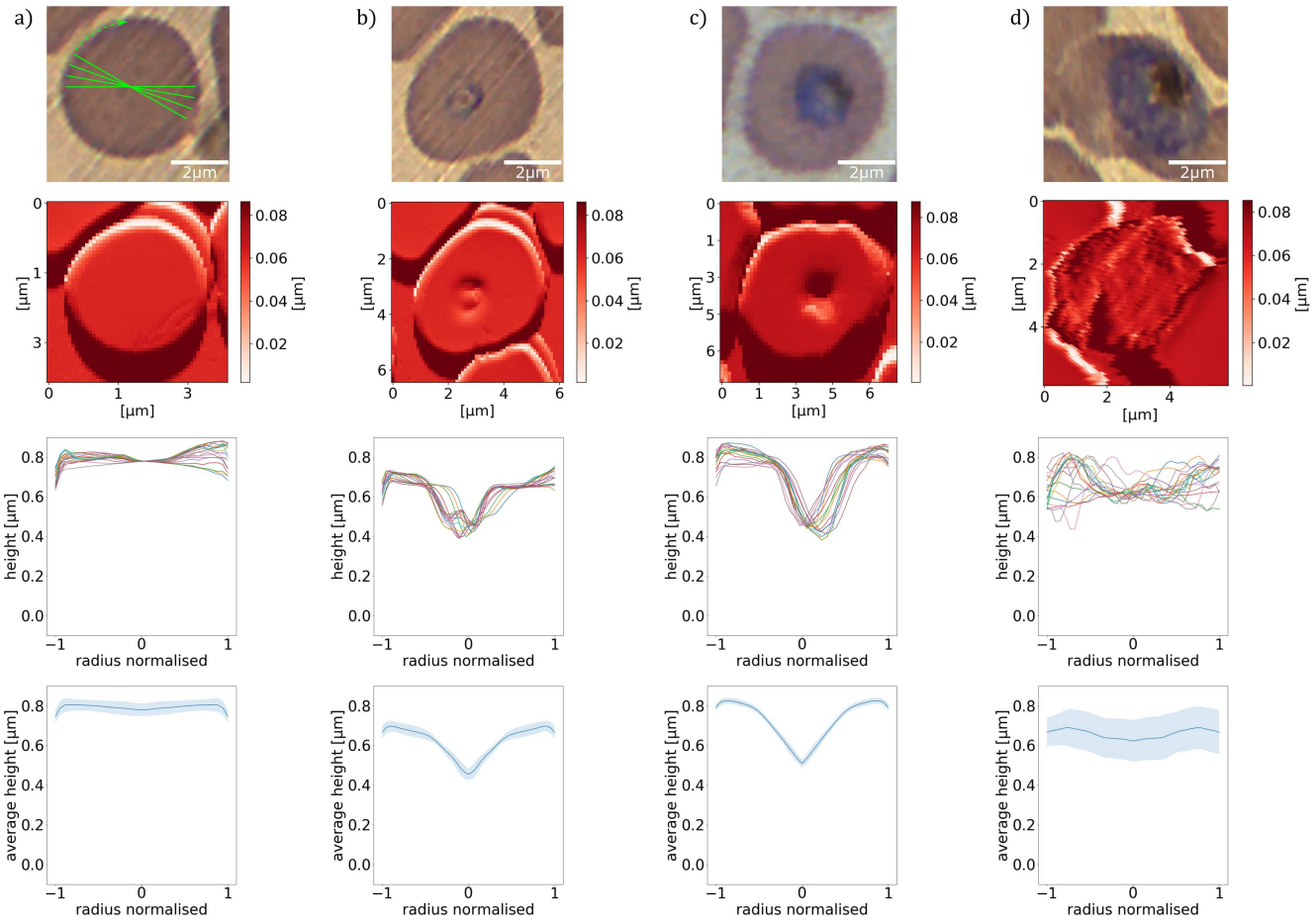

Figure 1. Morphology of RBCs infected by *P. falciparum*. Results on RBCs with no parasite, with ring, trophozoite and schizont stages are shown in columns (a), (b), (c) and (d), respectively. First row: BFM images of RBCs in stained smears. Second row: AFM topography images recorded over the same areas as the BFM images above. Third row: Radial height profiles of RBCs as obtained by radial cross-sections of the AFM topographic images, normalised to the radius of the cell. Green lines in the top-left panel indicate the path of the radial cross-sections. Forth row: Mean height profiles obtained by averaging the different cross-sections shown in the panels above. The standard deviation of the height is indicated by the shaded region around the curves.

the minimum near the centre h_{diff} shows a more pronounced dependence on the stages. The change in the height along the radius is ∼10%, ∼35%, ∼45% and ∼20% of the mean height for the uninfected RBC and for the ring, trophozoite and schizont stages, respectively. These values together with the values of the mean height are also displayed in Fig 3. Furthermore, the standard deviation of the height (indicated as a shaded area around the master curves) increases towards the centre in the trophozoite stage, while its radial dependence is weaker in the other three cases. Our observations show that these are valuable parameters to identify the developmental stages, comprising an essential part of the information encoded in the 2D images. Our methodological approach shows that statistical differences in the radial height profile of infected and an uninfected RBCs clearly classify the developmental stages. The extraction of characteristic parameters from the AFM images reveals a distinct pattern for each stage.

Fluorescence properties of *P. falciparum*

So far, we have shown that the topographical changes inhibited by the malaria parasite enable the classification of the developmental stages. Now, we will analyse if RBCs emit characteristic fluorescence in accordance with the maturation of the parasite and if this fluorescence pattern can be used to distinguish the stages. Maturation of the malaria parasite not only changes RBC structure, but also optical properties of the infected cell. In TIRF microscopy images (excitation wavelength 405 nm) of malaria-infected RBCs, foci of fluorescence emission appeared (Fig. 4). The 405 nm wavelength was chosen to be in

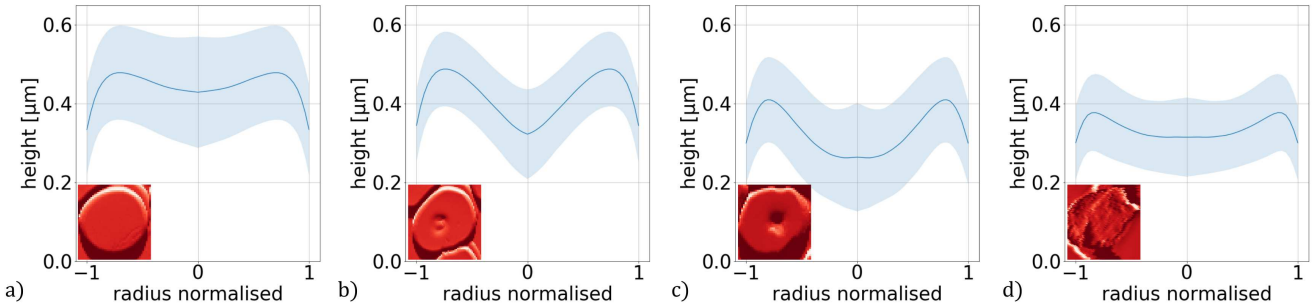

Figure 2. Height profiles of *P. falciparum*-infected RBCs. Master curves representing the typical height profiles of RBCs containing no parasites (a) and ring (b), trophozoite (c) and schizont (d) stages of *P. falciparum*. The height profile curves typical for a given stage were obtained by averaging the radial height profile curves of approx. 100 individual RBCs corresponding to the same stage. The shaded regions indicate the standard deviation. The radial height profile curves for individual RBCs are shown in the last row of Fig. 1.

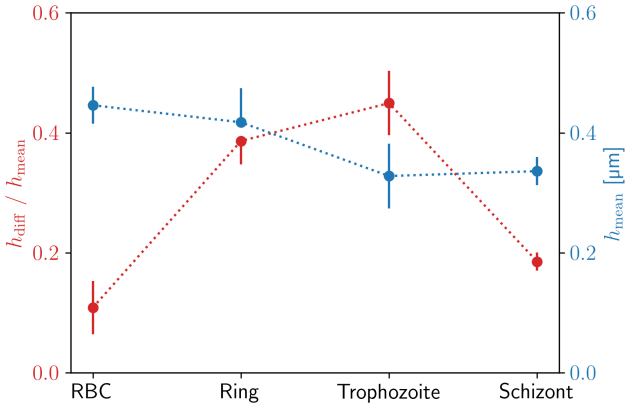

Figure 3. Characteristic identification pattern for height profiles of *P. falciparum* stages. Mean height of the RBCs and difference between maximum and minimum height divided by mean height along the radius for different developmental stages of *P. falciparum*. These parameters were calculated from the master curve of each stage, shown in Fig. 2.

resonance with the strongest absorption peak in protoporphyrin IX, which plays an important part in the heme biosynthesis[21,22]. Simultaneously we recorded BFM images on the same samples to identify the stage of the parasites. We observed that the fluorescence pattern changes with maturation. The uninfected RBC shows no fluorescence, as evident from the low and uniform signal in Fig. 4a, detected over the whole area of the cell. In the ring stage, a small spot with high fluorescence intensity is observed, which is connected to a more extended region of moderate fluorescence, embedded in the otherwise non-fluorescent cell (Fig. 4b). A central region in the trophozoite stage emits a diffuse signal surrounded by a non-fluorescent edge region of the cell (Fig. 4c). The diffuse region extends nearly over the cell diameter in the schizont stage, but quenching of the fluorescence is found close to the centre, visible as a dark spot in the middle of Fig. 4d. In fact, a similar non-fluorescent region, though smaller, can also be observed for the trophozoite stage. Based on the recorded fluorescence intensity profile, we performed a similar evaluation as for the topography in the AFM images. We cut the cell into radial cross-sections and plot the intensity of the TIRF images along these radial cuts. Figure 4 shows a TIRF image representative for each stage with the corresponding 2D intensity profiles. For an easier comparison with the AFM results, the spectra were inverted, so that the intensity increases from the top to the bottom. The intensity profiles closely resemble the height profiles of the infected RBCs (Fig. 1) and also show distinct patterns for each stage. Our analysis reveals characteristic fluorescence maps for each developmental stage. We found central non-fluorescent regions inside the trophozoite and schizont, where we expect the hemozoin crystals inside the food vacuole. As discussed later, the hemozoin is not the source of fluorescence in infected RBCs. However, the revelation of the molecular origin of fluorescence goes beyond the scope of the present study.

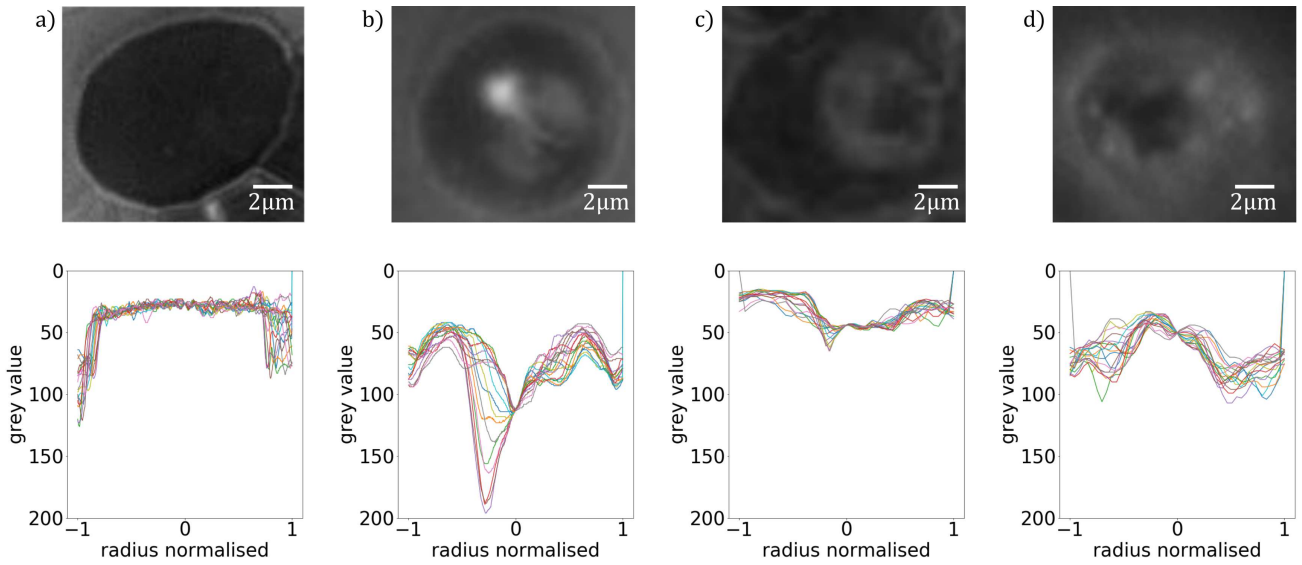

Figure 4. Fluorescence maps of RBCs infected with *P. falciparum*. Fluorescence properties of RBCs with no parasite (a), with ring (b), with trophozoite (c) and schizont (d) stage *P. falciparum* parasites, as studied by TIRF. First row: TIRF images of RBCs in thin smears. Second row: Radial fluorescence intensity profiles for the different stages, obtained as radial cross-sections of the images above.

Discussion

By combining AFM, TIRF and BFM, here we characterised the developmental stages of *P. falciparum* parasites in thin smears of synchronized cultures. Our data demonstrate that the maturation of the parasite not only changes the morphology of the RBC but also results in the emergence of fluorescence emission. With a statistical analysis of the height profiles of the cells, we could derive an identification pattern for each developmental stage. The average height together with the maximum height difference and the standard deviation of the master curves clearly characterise the stages. Our results on morphology support the observations reported about the maturation of malaria parasites by Grüring *et al.*[8]. While the uninfected RBC, the ring and schizont stages are rather symmetrical to the centre of the cell, the symmetry is usually disrupted in the trophozoite stage. Grüring *et al.* showed that the food vacuole settles to the side of the trophozoite, which might explain the asymmetric behaviour of the height profiles in Fig. 5a. With maturation into the schizont stage, they observed a shifting of the food vacuole back to a more central position[8]. Therefore, the central peak we measured in the height profile of the schizont, as shown in Fig. 5b, is likely to be the food vacuole.

The combined BF and TIRF imaging provided new information about the autofluorescence properties of malaria parasites. We could show that uninfected cells emit no detectable fluorescence when excited at 405 nm, while fluorescence emission can be detected in infected RBCs during maturation. The signal changed from a well defined indentation in the ring stage to a diffuse pattern in the schizont stage. In the signal of the trophozoite (Fig. 6a and b, middle) and schizont stage (Fig. 6a and b, right), we identified non-fluorescent regions inside the fluorescent parasite. An additional TIRF study on extracted hemozoin crystals showed no fluorescence emission (Fig. 6a and b, left). This highly suggests that we can image malaria pigment with TIRF. However, it is important to note that TIRF is a surface sensitive method with a penetration depth of $\sim 200\,\mathrm{nm}$[23]. Such signatures of the food vacuole can indeed be resolved in the other exemplary AFM images of trophozoite and schizont stages in Fig. 1c & d, though less pronouncedly in the schizont stage.

When comparing the fluorescence maps with the topography images, respectively shown in the bottom line of Fig. 4 and the third row of Fig. 1, we observe a clear correlation: The features characteristic to the different parasite stages appear in the two types of images in a similar fashion. Most interestingly, our hypothesis that the central peak observed in the height profiles for trophozoites and schizonts corresponds to the food vacuole is supported by TIRF studies on the same stages. Figs. 6b & c display BFM and TIRF images simultaneously recorded on RBCs containing trophozoites and schizonts, respectively. The food vacuole appears as a dark spot within the parasite in both cases. The non-fluorescent nature of hemozoin is evident in Figs. 6a by TIRF microscopy on extracted hemozoin crystals. We believe that the darkness of the food vacuole is caused by self-quenching of chemically identical fluorophores. However, the source of fluorescence is not clear.

Our experiments clearly illustrate the connection between RBC morphology, fluorescence properties and the maturation

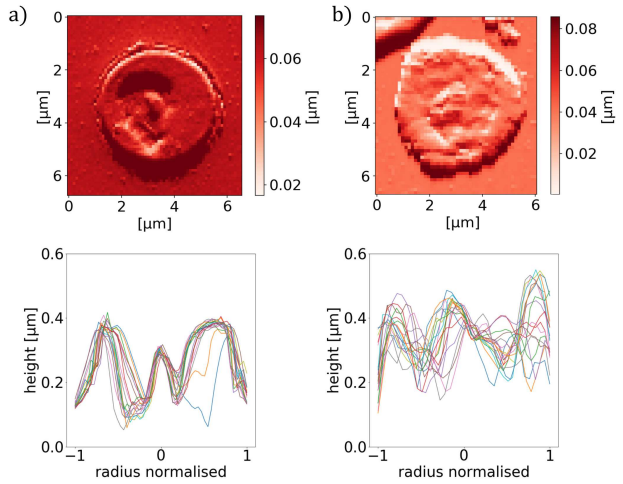

Figure 5. Characteristic cross-sections of *P. falciparum*-infected RBCs. AFM images (top panels) and the corresponding radial cross-sections of the height (bottom panels) for a RBC containing a trophozoite/schizont in column (a)/(b). The cross-section shows a maximum around the centre of the cell in both cases.

of *P. falciparum* and these observations can help to establish structure–function relations, to reveal the detailed mechanisms governing the intracellular parasite activity and eventually to guide the development of new antimalarials. From the statistical difference in the radial height profile of RBCs, we could derive identification patterns characteristic to the different parasite stages. These closely correlate with typical fluorescence maps of the cells. Furthermore, the topographical and optical features provide a tool to locate hemozoin crystals. Revealing connections between the structure and the hemozoin content of RBCs, and their consequences on the optical properties are highly relevant for recent diagnostic schemes targeting at hemozoin, like the rotating-crystal magneto-optical diagnosis[6,7].

Nevertheless, the present study, performed on fixed cells, has some inherent limitations. Under such conditions, the shape of the RBCs is deformed, i.e. the cells are flattened, and their mechanical properties are also altered by partial dehydration. Furthermore, the smears only show a snapshot of the parasite life cycle. By extending the experiments to living parasites, more detailed and realistic information about the parasite maturation can be obtained. However, performing multi-probe imaging under conditions close to those in the human body requires simultaneous liquid AFM and TIRF studies on parasite cultures, which is a highly challenging task.

Methods

Sample preparation

P. falciparum parasites from the laboratory adapted strain 3D7 were cultured in culture medium (Albumax, 25 mg/L Gentamycin, RPMI 1640) and maintained in an atmosphere of 5 % CO_2 and 5 % O_2 as in previous studies[4,5,24]. The cultures were raised to 5 % parasitemia and treated with Percoll or Sorbitol to synchronise the parasites. For the AFM measurements, we sorted the schizont stage parasites from other stages. For this, cultured parasites were added to 5 ml of Percoll and centrifuged, layering them according to their densities. The schizonts, having the smallest density of the developmental stages, could be recovered from the first layer[25]. After centrifugation, 1.2 µl of the remaining pellet of RBCs with enriched parasitemia were used to make a thin film smear on a glass slide. This procedure was repeated for ring stage parasites, which were sorted by Sorbitol treatment[16].
To classify the parasites prior to the morphology measurement, the smears were stained with Giemsa's stain[17].

Morphological measurements

For the morphological measurements of the smears, we used an MFP-3D AFM (Asylum Research, Oxford Instruments). It was operated in AC mode at a scanning speed of 0.25 Hz. Scan areas of 90 x 90 µm were collected to analyse the morphology of RBCs. Each scan was performed with a resolution of 512 x 512 pixels.

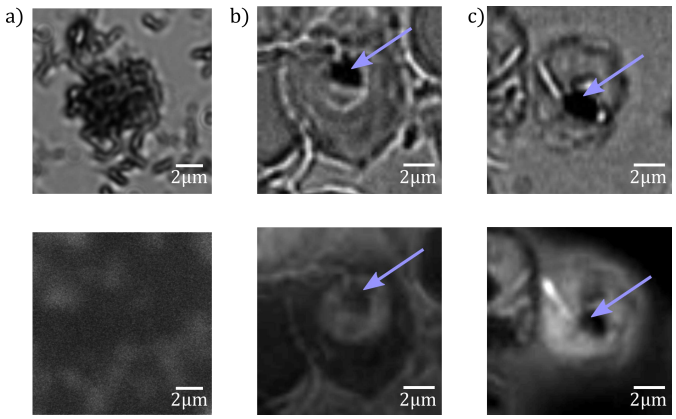

Figure 6. Fluorescence maps of hemozoin crystals. BFM (top panels) and TIRF (bottom panels) images of extracted hemozoin crystals in column (a) and of RBCs containing a trophozoite and schizont in column (b) and (c), respectively. The extracted hemozoin crystals show no fluorescence. In the trophozoite and schizont, the non-fluorescent regions are indicated by blue arrows.

Fluorescence measurements

For the analysis of fluorescence properties of *P. falciparum*, we used a TIRF microscope, which was operated at a wavelength of 405 nm. The smears were prepared on a cover slip and dried in air before the measurement.

Evaluation program

The data we analysed was obtained from the height trace and the amplitude of each AFM scan. By thresholding the original data, we were able to detect all cells in the scan. To characterise the cells by height profile, we determined 18 cross-sections through the height trace, which were rotated in the cell plane by an angle of 10°, so that every pixel along the outline of the cell was covered. To describe a single cell, radial sections through the cell were averaged by height.

References

1. Organization World Health. Malaria. https://www.who.int/news-room/fact-sheets/detail/malaria (2019).
2. White, N. J. Malaria. In *Manson's tropical infectious diseases*, 43, chap. 9, 532–600, DOI: 10.1016/S0140-6736(18)30324-6 (Saunders Ltd., 2014), 23 edn.
3. Lilley, K. & al, E. *Malaria microscopy* (World Health Organization, 2015), 2 edn.
4. Orbán, Á. *et al.* Evaluation of a novel magneto-optical method for the detection of malaria parasites. *PLoS ONE* **9**, 1–8, DOI: 10.1371/journal.pone.0096981 (2014).
5. Orban, A. *et al.* Efficient monitoring of the blood-stage infection in a malaria rodent model by the rotating-crystal magneto-optical method. *Sci. Reports* **6**, 1–9, DOI: 10.1038/srep23218 (2016).
6. Butykai, A. *et al.* Malaria pigment crystals as magnetic micro-rotors: Key for high-sensitivity diagnosis. *Sci. Reports* **3**, 1–10, DOI: 10.1038/srep01431 (2013). 1210.5920.
7. Arndt, L. *et al.* Magneto-optical diagnosis of symptomatic malaria in Papua New Guinea. *Nat. Commun.* **969**, 1–10, DOI: 10.1038/s41467-021-21110-w (2021).
8. Grüring, C. *et al.* Development and host cell modifications of Plasmodium falciparum blood stages in four dimensions. *Nat. communications* DOI: 10.1038/ncomms1169 (2011).
9. Nagao, E., Kaneko, O. & Dvorak, J. A. Plasmodium falciparum-infected erythrocytes: Qualitative and quantitative analyses of parasite-induced knobs by atomic force microscopy. *J. Struct. Biol.* **130**, 34–44, DOI: 10.1006/jsbi.2000.4236 (2000).
10. Shi, H. *et al.* Life Cycle-Dependent Cytoskeletal Modifications in Plasmodium falciparum Infected Erythrocytes. *PLoS ONE* **8**, 1–10, DOI: 10.1371/journal.pone.0061170 (2013).
11. Perez-Guaita, D. *et al.* Multispectral Atomic Force Microscopy-Infrared Nano-Imaging of Malaria Infected Red Blood Cells. *Anal. Chem.* **90**, 3140–3148, DOI: 10.1021/acs.analchem.7b04318 (2018).

12. Masilamani, V. *et al.* Fluorescence spectral diagnosis of malaria – a preliminary study. *Diagn. Pathol.* 1–7, DOI: 10.1186/s13000-014-0182-z (2014).

13. Opoku-ansah, J., Eghan, M. J., Anderson, B., Boampong, J. N. & Buah-bassuah, P. K. Laser-Induced Autofluorescence Technique for Plasmodium falciparum Parasite Density Estimation. *Appl. Phys. Res.* **8**, 43–51, DOI: 10.5539/apr.v8n2p43 (2016).

14. Nanoscience Instruments. Atomic force microscopy. https://www.nanoscience.com/techniques/atomic-force-microscopy/ (2019).

15. Scudiero, L. *et al.* Comparisons of the topographic characteristics and electrical charge distributions among Babesia-infected erythrocytes and extraerythrocytic merozoites using AFM. *J. Microsc.* **271**, 84–97, DOI: 10.1111/jmi.12697 (2018).

16. Ross, S. T., Schwartz, S., Fellers, T. J. & Davidson, M. W. Total internal reflection fluorescence (TIRF) microscopy. https://www.microscopyu.com/techniques/fluorescence/total-internal-reflection-fluorescence-tirf-microscopy (2019).

17. Shute, P. E. & Maryon, M. E. *Laboratory technique for the study of malaria* (J. & A. Churchill, London, 1960), 2nd edn.

18. Kasetsirikul, S., Buranapong, J., Srituravanich, W., Kaewthamasorn, M. & Pimpin, A. The development of malaria diagnostic techniques: A review of the approaches with focus on dielectrophoretic and magnetophoretic methods. *Malar. J.* **15**, 358, DOI: 10.1186/s12936-016-1400-9 (2016).

19. Kollipara, P. IR Spectroscopy quickly detects malaria at early stages. https://cen.acs.org/articles/92/web/2014/04/IR-Spectroscopy-Quickly-Detects-Malaria.html (2014).

20. Diez-Silva, M., Dao, M., Han, J., Lim, C.-T. & Suresh, S. Shape and Biomechanical Characteristics of Human Red Blood Cells in Health and Disease. *MRS bulletin / Mater. Res. Soc.* **35**, 382–388, DOI: 10.1557/mrs2010.571 (2010).

21. Hennig, G. *et al.* Dual-wavelength excitation for fluorescence-based quantification of zinc protoporphyrin IX and protoporphyrin IX in whole blood. *J. Biophotonics* **524**, 514–524, DOI: 10.1002/jbio.201200228 (2014).

22. Roberts, D. W. *et al.* Red-light excitation of protoporphyrin IX fluorescence for subsurface tumor detection. *J. Neurosurg.* **128**, 1690–1697, DOI: 10.3171/2017.1.JNS162061.1690 (2018).

23. Ockenga, W. Total internal reflection fluorescence (TIRF) (2012).

24. Trager, W. & Jensen, J. Human malaria parasites in continuous culture. *Science* **193**, 673–675 (1976).

25. Rivadeneira, E. M., Wasserman, M. & Espinal, C. T. Separation and Concentration of Schizonts of Plasmodium falciparum by Percoll Gradients. *The J. Protozool.* **30**, 367–370, DOI: 10.1111/j.1550-7408.1983.tb02932.x (1983).

Acknowledgements

The research carried out here was supported by the National Research, Development and Innovation Office of Hungary (K119493, VEKOP-2.3.2-16-2017-00013 to BGV, NKP-2018-1.2.1-NKP-2018-00005), the BME-Biotechnology FIKP grant of EMMI (BME FIKP-BIO), the BME-Nanotechnology and Materials Science FIKP grant of EMMI (BME FIKP-NAT), the National Heart Programme (NVKP-16-1-2016-0017), K124966 and K135360 to MK, National Bionics Programme ED_17-1-2017-0009 and SE FIKP-Therapy Grant.

Author contributions statement

K.P. and P.M. cultured the parasites and prepared the samples. K.P. and M.K. performed the experiment, K.P. analysed the data. All authors contributed to the discussion and writing of the manuscript. I.K. and M.K. supervised the project. All authors reviewed the manuscript.

Additional information

Competing interests The authors declare no competing interests.

Figures

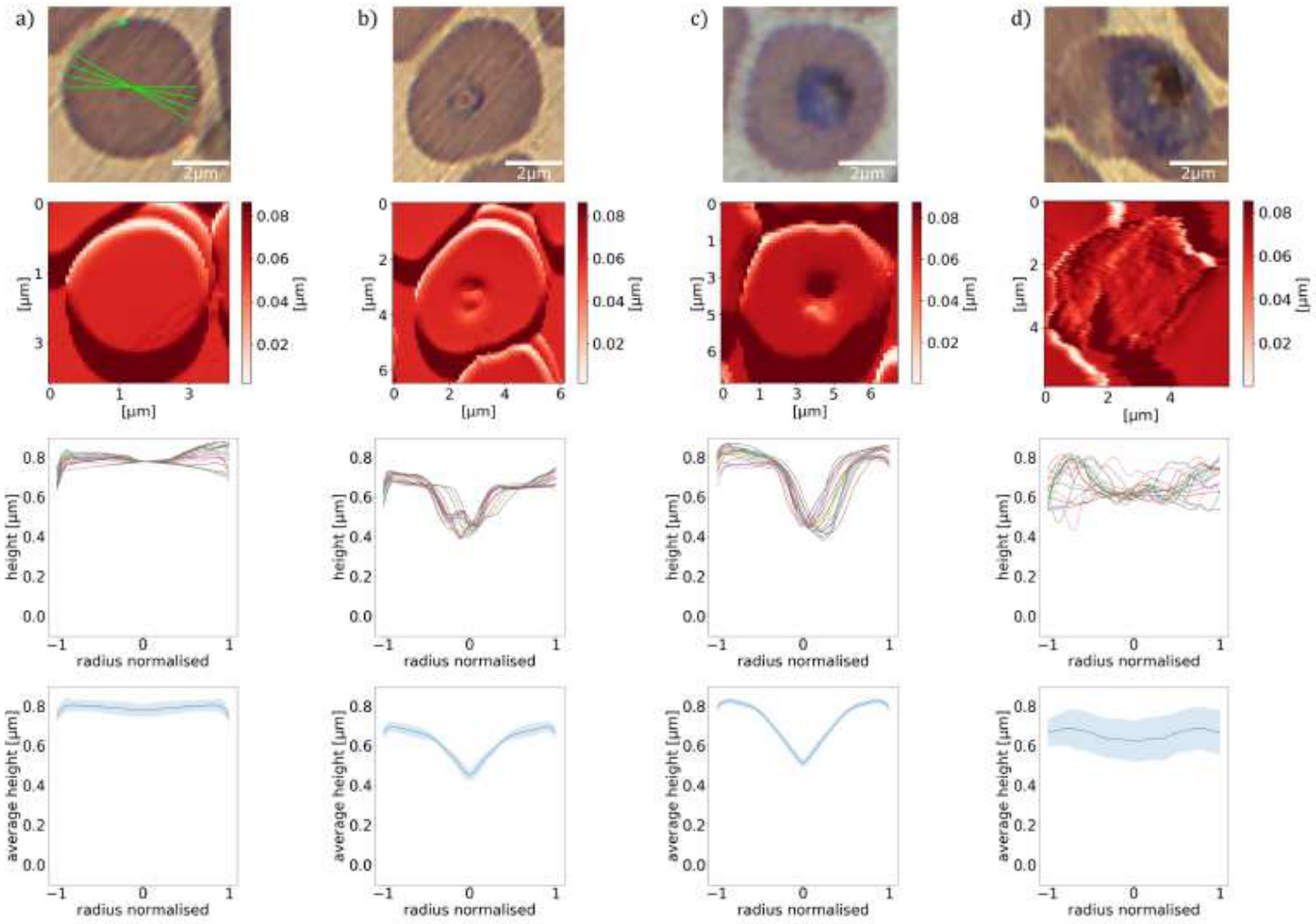

Figure 1

Morphology of RBCs infected by P. falciparum. Results on RBCs with no parasite, with ring, trophozoite and schizont stages are shown in columns (a), (b), (c) and (d), respectively. First row: BFM images of RBCs in stained smears. Second row: AFM topography images recorded over the same areas as the BFM images above. Third row: Radial height profiles of RBCs as obtained by radial cross-sections of the AFM topographic images, normalised to the radius of the cell. Green lines in the top-left panel indicate the path of the radial cross-sections. Forth row: Mean height profiles obtained by averaging the different cross-sections shown in the panels above. The standard deviation of the height is indicated by the shaded region around the curves.

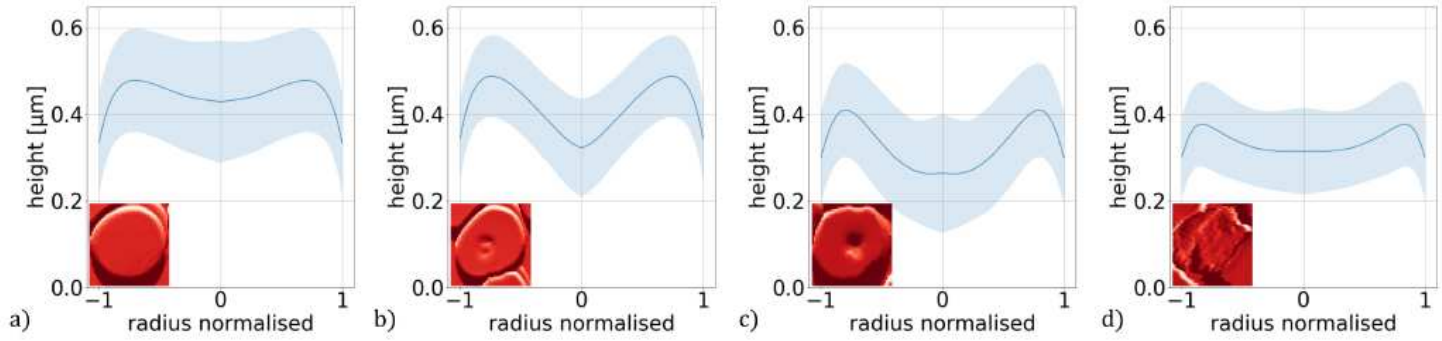

Figure 2

Height profiles of P. falciparum-infected RBCs. Master curves representing the typical height profiles of RBCs containing no parasites (a) and ring (b), trophozoite (c) and schizont (d) stages of P. falciparum. The height profile curves typical for a given stage were obtained by averaging the radial height profile curves of approx. 100 individual RBCs corresponding to the same stage. The shaded regions indicate the standard deviation. The radial height profile curves for individual RBCs are shown in the last row of Fig. 1.

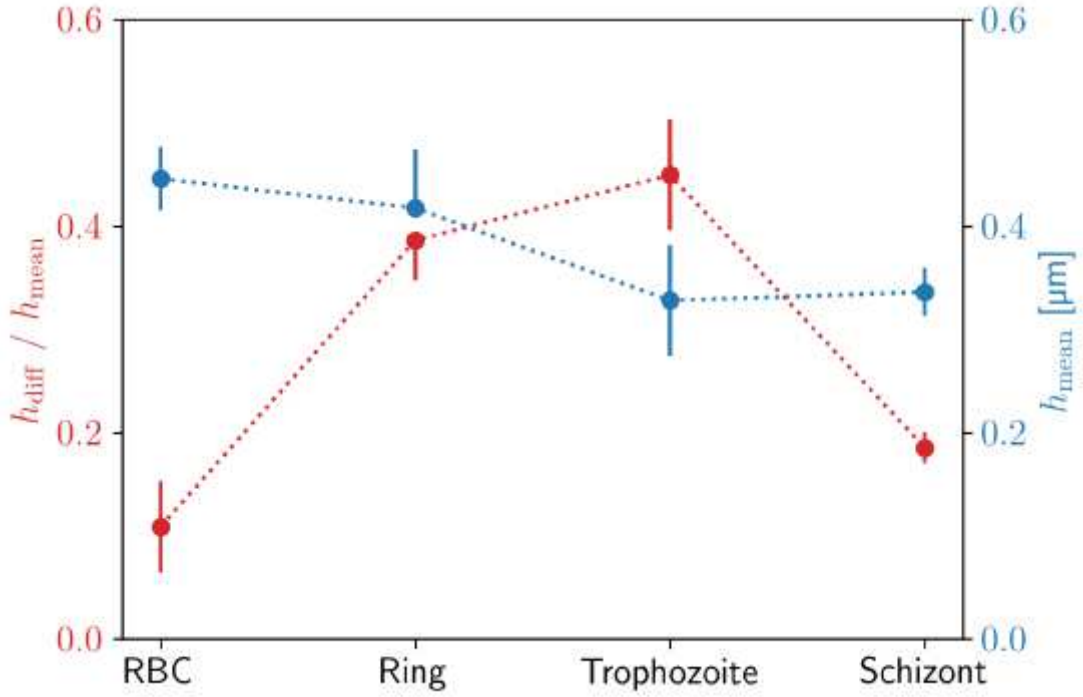

Figure 3

Characteristic identification pattern for height profiles of P. falciparum stages. Mean height of the RBCs and difference between maximum and minimum height divided by mean height along the radius for different developmental stages of P. falciparum. These parameters were calculated from the master curve of each stage, shown in Fig. 2.

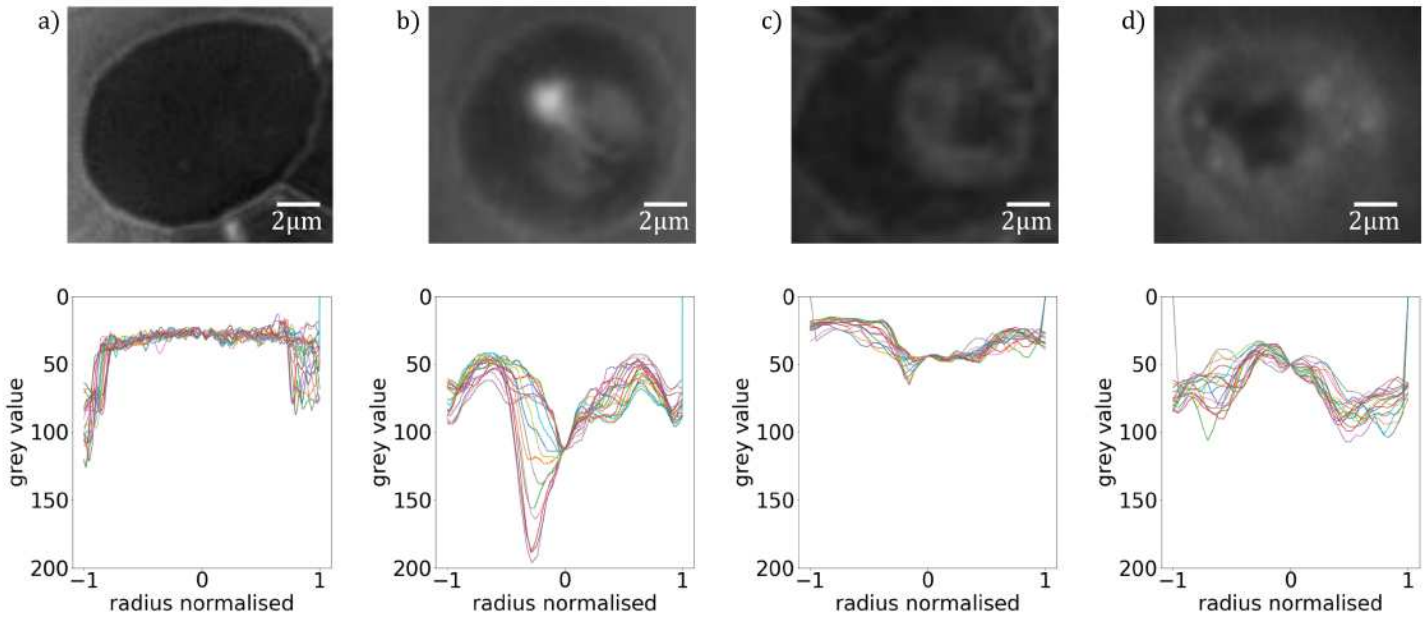

Figure 4

Fluorescence maps of RBCs infected with P. falciparum. Fluorescence properties of RBCs with no parasite (a), with ring (b), with trophozoite (c) and schizont (d) stage P. falciparum parasites, as studied by TIRF. First row: TIRF images of RBCs in thin smears. Second row: Radial fluorescence intensity profiles for the different stages, obtained as radial cross-sections of the images above.

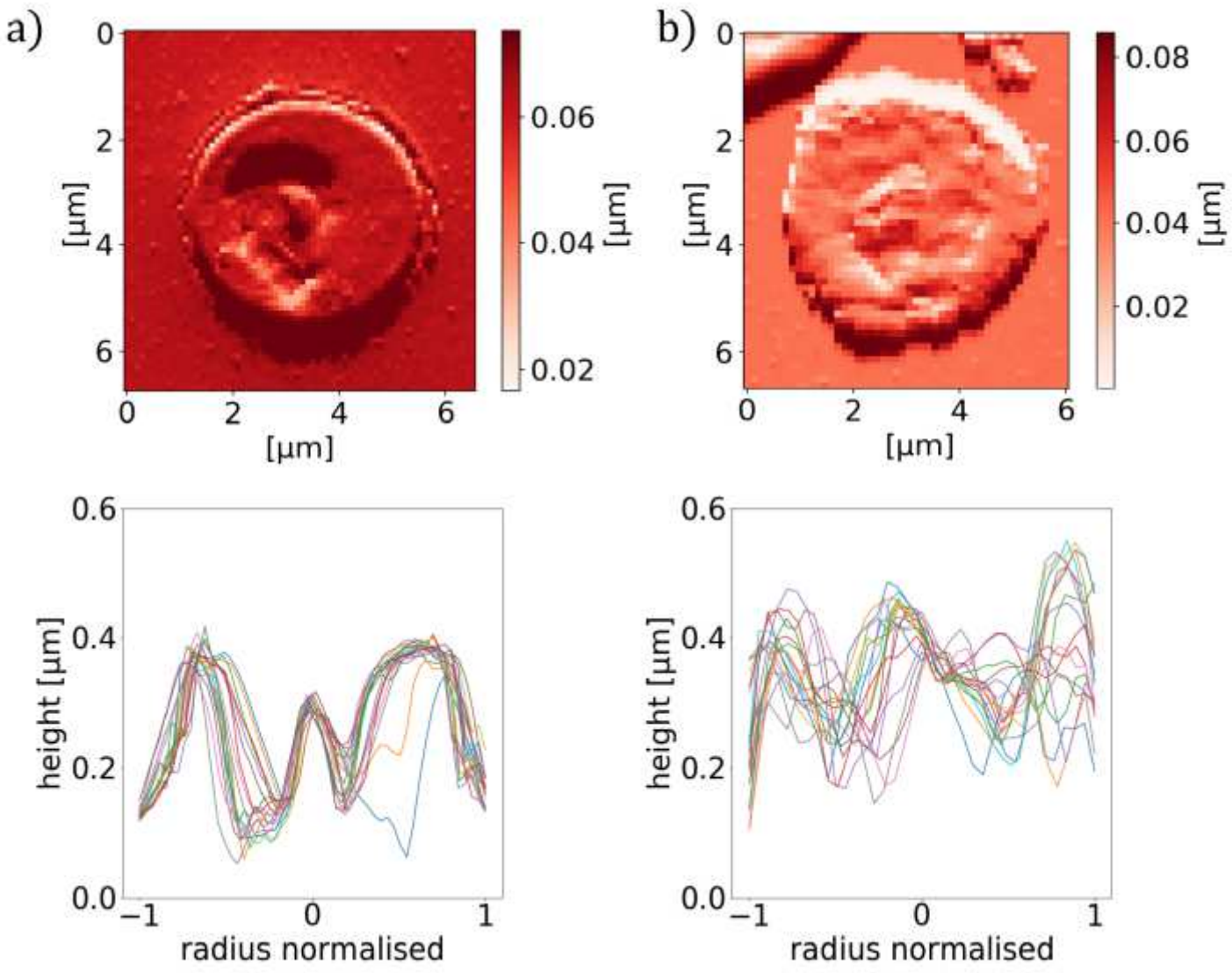

Figure 5

Characteristic cross-sections of P. falciparum-infected RBCs. AFM images (top panels) and the corresponding radial cross-sections of the height (bottom panels) for a RBC containing a trophozoite/schizont in column (a)/(b). The cross-section shows a maximum around the centre of the cell in both cases.

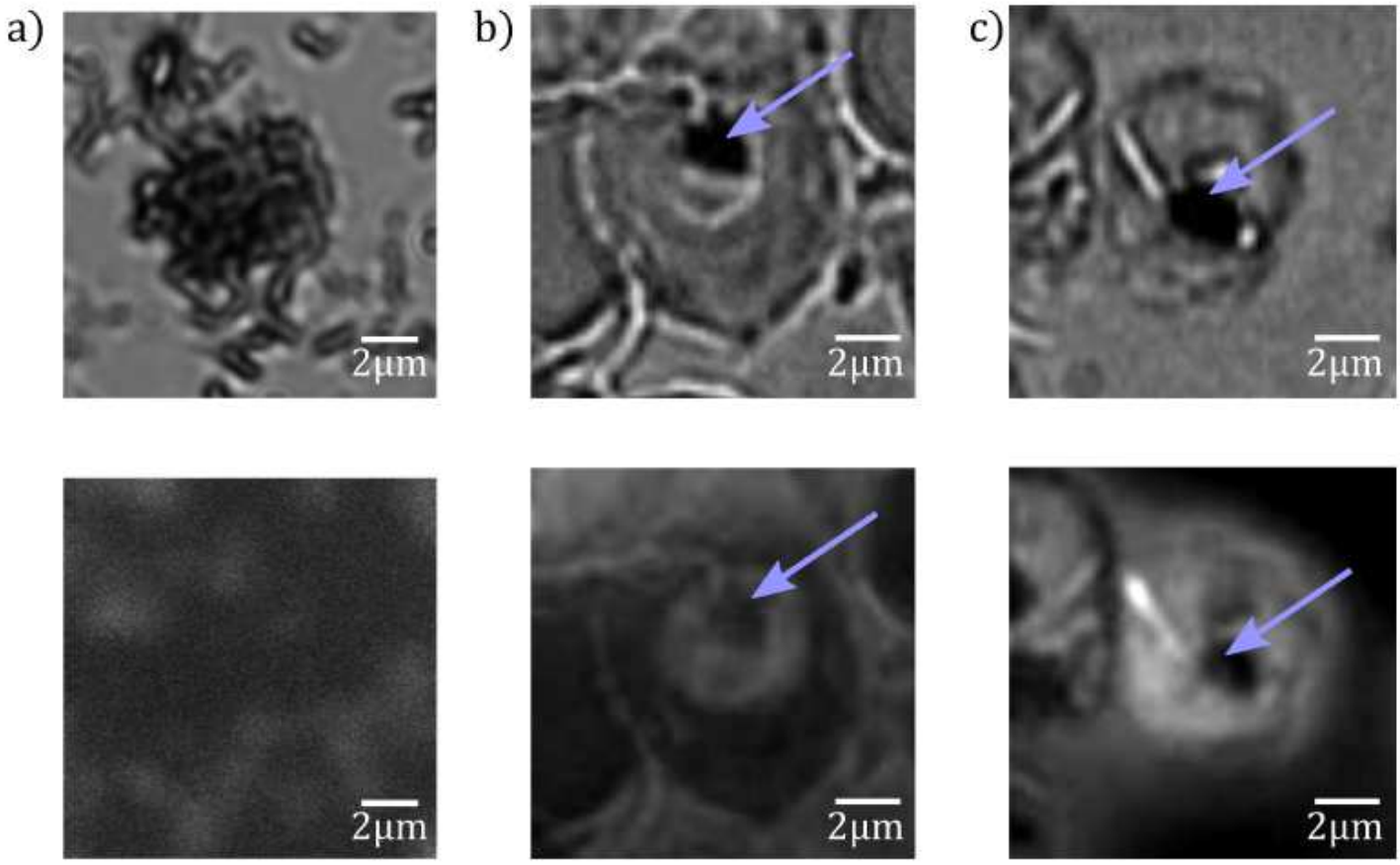

Figure 6

Fluorescence maps of hemozoin crystals. BFM (top panels) and TIRF (bottom panels) images of extracted hemozoin crystals in column (a) and of RBCs containing a trophozoite and schizont in column (b) and (c), respectively. The extracted hemozoin crystals show no fluorescence. In the trophozoite and schizont, the non-fluorescent regions are indicated by blue arrows.